

# A Modular, Dynamic, DNA-Based Platform for Regulating Cargo Distribution and Transport between Lipid Domains

Roger Rubio-Sánchez, Simone Eizagirre Barker, Michal Walczak, Pietro Cicuta, and Lorenzo Di Michele\*



Cite This: *Nano Lett.* 2021, 21, 2800–2808



Read Online

ACCESS |



Metrics & More



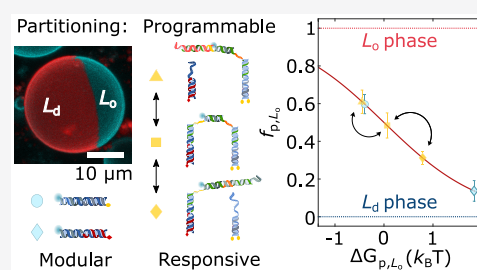
Article Recommendations



Supporting Information

**ABSTRACT:** Cell membranes regulate the distribution of biological machinery between phase-separated lipid domains to facilitate key processes including signaling and transport, which are among the life-like functionalities that bottom-up synthetic biology aims to replicate in artificial-cellular systems. Here, we introduce a modular approach to program partitioning of amphiphilic DNA nanostructures in coexisting lipid domains. Exploiting the tendency of different hydrophobic “anchors” to enrich different phases, we modulate the lateral distribution of our devices by rationally combining hydrophobes and by changing nanostructure size and topology. We demonstrate the functionality of our strategy with a bioinspired DNA architecture, which dynamically undergoes ligand-induced reconfiguration to mediate cargo transport between domains via lateral redistribution. Our findings pave the way to next-generation biomimetic platforms for sensing, transduction, and communication in synthetic cellular systems.

**KEYWORDS:** DNA nanotechnology, lipid phase separation, lipid domains, partitioning, artificial cells, synthetic membranes, biomimicry



Biological membranes are highly heterogeneous, containing up to 20% of the protein content of a cell and featuring hundreds of different lipid species.<sup>1,2</sup> Such a degree of complexity evolved alongside the myriad of biological processes hosted and regulated by membranes, which include signaling, adhesion, trafficking, motility, and division.<sup>3</sup> Many of these functionalities rely on lateral colocalization of membrane proteins<sup>4</sup> required for the emergence of signaling hubs,<sup>5,6</sup> focal adhesions,<sup>7</sup> and assemblies regulating membrane architecture to promote endo- and exocytosis<sup>8</sup> and cell division.<sup>9</sup>

Cells have evolved a variety of active and passive mechanisms to regulate the local composition of their membranes, overcoming the extreme molecular heterogeneity.<sup>10–12</sup> Among these, proteolipid phase separation is thought to play an important role in signaling and signal transduction.<sup>13</sup> In this process, nanoscale domains or *rafts* are believed to emerge, rich in sphingomyelins and sterols, which are able to recruit or exclude membrane proteins based on their different affinities for raft and non-raft environments.<sup>14,15</sup>

Bottom-up synthetic biology aims at replicating functionalities typically associated with biological cells in microrobots designed *de novo* or “artificial cells”.<sup>16–18</sup> Just like their biological counterparts, many artificial-cell designs rely on semipermeable membranes for their compartmentalization requirements,<sup>19–21</sup> which can be constructed from polymers<sup>22</sup> and proteopolymer systems,<sup>23,24</sup> colloids<sup>25,26</sup> and, more often, synthetic lipid bilayers.<sup>21</sup> However, with some remarkable exceptions,<sup>27–31</sup> reviewed in ref 32, the membranes of artificial cells are often passive enclosures, lacking the complex

functionalities of biological interfaces. A precise control over the local molecular makeup of synthetic lipid bilayers is therefore highly desirable and a necessary stepping stone for the development of ever more sophisticated life-like responses in artificial cells.

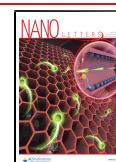
DNA nanotechnology has demonstrated great potential as a means of creating responsive nanostructures that emulate biological architectures and functionalities and are becoming increasingly popular constituents of artificial cellular systems.<sup>33,34</sup> In many cases, biomimetic DNA nanostructures, rendered amphiphilic by hydrophobic tags, have been interfaced to synthetic lipid membranes to replicate the response of cell-membrane machinery. Examples include DNA architectures mediating artificial cell adhesion and tissue formation,<sup>35–41</sup> regulating transport,<sup>42,43</sup> enabling signal transduction,<sup>44</sup> and tailoring membrane curvature.<sup>45,46</sup>

Importantly, amphiphilic DNA nanostructures have been demonstrated to undergo preferential partitioning when anchored to phase-separated synthetic bilayers, an effect that is reminiscent of membrane-protein partitioning in *rafts*.<sup>47–49</sup> The preference of DNA nanostructures for different lipid phases and their degree of partitioning have been shown to

**Received:** December 10, 2020

**Revised:** March 3, 2021

**Published:** March 18, 2021



ACS Publications

© 2021 The Authors. Published by  
American Chemical Society

2800

<https://doi.org/10.1021/acs.nanolett.0c04867>  
*Nano Lett.* 2021, 21, 2800–2808

depend on the chemical identity of the hydrophobic anchors, membrane lipid composition, temperature, and solvent conditions.<sup>40,50</sup> For instance, in ternary model membranes of 1,2-dioleoyl-*sn*-glycero-3-phosphocholine (DOPC)/1,2-dipalmitoyl-*sn*-glycero-3-phosphocholine (DPPC)/cholesterol displaying coexistence of liquid ordered ( $L_o$ ) and liquid disordered ( $L_d$ ) phases,<sup>1,51,52</sup> DNA constructs bearing a single cholesteryl-tri(ethylene glycol) (TEG) anchor show a weak preference for  $L_o$ , while duplexes end-functionalized with two cholesteryl-TEG anchors partition in  $L_o$  more prominently.<sup>53,54</sup> Conversely, oligonucleotides functionalized with  $\alpha$ -tocopherol preferentially localize within the  $L_d$  phases of ternary 1-palmitoyl-2-oleoyl-*sn*-glycero-3-phosphocholine (POPC)/sphingomyelin (SM)/cholesterol membranes.<sup>55,56</sup> Moreover, dynamic control over the partitioning has also been exemplified with DNA nanodevices that redistribute between lipid phases following enzymatic cleavage<sup>57</sup> or changes in ionic strength.<sup>58</sup>

The ability to influence partitioning of membrane-anchored DNA constructs makes them promising tools for engineering the molecular makeup and functionality of artificial cell membranes. Yet, we have effectively only started to scratch the surface of the massive design space of amphiphilic DNA nanostructures that, alongside the chemical identity of the hydrophobes, can be freely engineered with respect to their size, topology, and stimuli responsiveness.

Here we introduce a modular platform that fully exploits the design versatility of DNA nanotechnology to construct nanostructures whose ability to partition in the domains of phase-separated synthetic membranes can be precisely programmed. Besides enabling static membrane patterning, the nanodevices can be dynamically reconfigured upon exposure to molecular cues, triggering redistribution between domains and unlocking synthetic pathways for cargo transport, signaling and morphological adaptation in synthetic cellular systems.

Our nanostructures were constructed from synthetic DNA oligonucleotides, some of which were covalently linked to hydrophobic moieties to mediate anchoring to the membrane. Fluorescent tags (Alexa488, unless stated otherwise) were also included to monitor the distribution of the nanostructures via confocal microscopy. As depicted in Figure 1 (left), we decorated the outer leaflet of phase-separated giant unilamellar vesicles (GUVs) with the DNA constructs. Unless specified otherwise, GUVs were prepared from ternary lipid mixtures (DOPC/DPPC/cholesterol) to display  $L_d$ – $L_o$  coexistence. To enable fluorescence imaging, the vesicles were doped at 0.8% molar ratio with TexasRed-DHPE, which preferentially labels the  $L_d$  phase. At room temperature, the GUVs readily de-mixed into two macroscopic  $L_o$  and  $L_d$  domains. The resulting Janus-like morphology, shown in Figure 1 (right), enabled the facile visualization and quantitation of the lateral distribution of the nanostructures.

To this end, equatorial confocal micrographs of the GUVs were collected and analyzed with a custom-built image processing pipeline, as described in detail in the SI (see Methods, and the associated Figures S1 and S2), which determined the average fluorescence intensities of the constructs in the two phases:  $I_{L_o}$  and  $I_{L_d}$ . From these values, fractional intensities  $f_{p,L_o(L_d)} = I_{L_o(L_d)} / (I_{L_o} + I_{L_d})$  were extracted. Throughout this letter, we refer to the fractional fluorescence intensity of nanostructures in the  $L_o$  phase,  $f_{p,L_o}$ , to gauge their

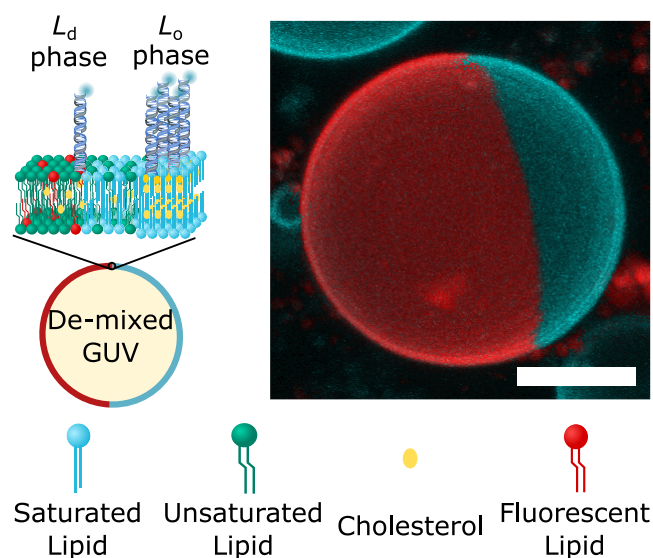


**Figure 1.** Membrane-anchored DNA nanostructures display preferential partitioning between the phases of de-mixed giant unilamellar vesicles. (left) Schematic representation of a multicomponent giant unilamellar vesicle (GUV), prepared with saturated and unsaturated lipids mixed with sterols, displaying liquid-ordered ( $L_o$ ) and liquid-disordered ( $L_d$ ) phase coexistence. The outer leaflet of the membrane is functionalized with amphiphilic DNA nanostructures, exemplified here with constructs bearing two cholesterol anchors, which enrich their preferred ( $L_o$ ) phase. (right) 3D view of a de-mixed GUV from confocal z-stack as obtained from Volume viewer (FIJI<sup>59</sup>) using maximum projection. DNA nanostructures (cyan) partition to the  $L_o$  domain, while the  $L_d$  phase (red) is labeled with TexasRed-DHPE. Scale bar = 10  $\mu$ m.

partitioning tendency. Förster resonance energy transfer (FRET) between Alexa488 on the DNA and TexasRed on the lipids, alongside fluorescent-signal cross-talk, could in principle bias  $f_{p,L_o}$  in certain partitioning states. To rule out this possibility, we performed dedicated experiments to determine the impact of both potential artifacts, as well as controls on GUVs that lack the TexasRed fluorophore, thus altogether eliminating the possible source of bias. Data in Figure S3, and the associated Supplementary Discussion 1, confirm that FRET and fluorescence cross-talk carry a negligible impact on  $f_{p,L_o}$ .

Assuming that the recorded fluorescence intensities are proportional to nanostructure concentrations, a partitioning free energy can be calculated as  $\Delta G_{p,L_o} = -k_B T \log(f_{p,L_o}/f_{p,L_d})$ . The latter is defined as the free energy change associated with relocating a single construct from the  $L_d$  to the  $L_o$  phase.

First, we applied our data-analysis pipeline on simple DNA duplexes featuring well characterized single cholesterol-TEG (sC) or single tocopherol (sT) anchors, as summarized in Figure 2. Expectedly, while sC anchors led to a marginal  $L_o$ -preference ( $f_{p,L_o}^{\text{sC}} \approx 0.6$ ,  $\Delta G_{p,L_o}^{\text{sC}} \approx -0.4k_B T$ ), nanostructures featuring sT strongly partitioned in  $L_d$  ( $f_{p,L_o}^{\text{sT}} \approx 0.14$ ,  $\Delta G_{p,L_o}^{\text{sT}} \approx 1.9k_B T$ ).

Importantly, as highlighted in Figure S4, the size heterogeneity of electroformed GUVs does not affect the lateral distribution of DNA anchored species, as  $f_{p,L_o}$  does not correlate with vesicle radius.

The substantial difference in the partitioning behaviors induced by sT and sC traces a route to program lateral distribution by combining multiple or different hydrophobic

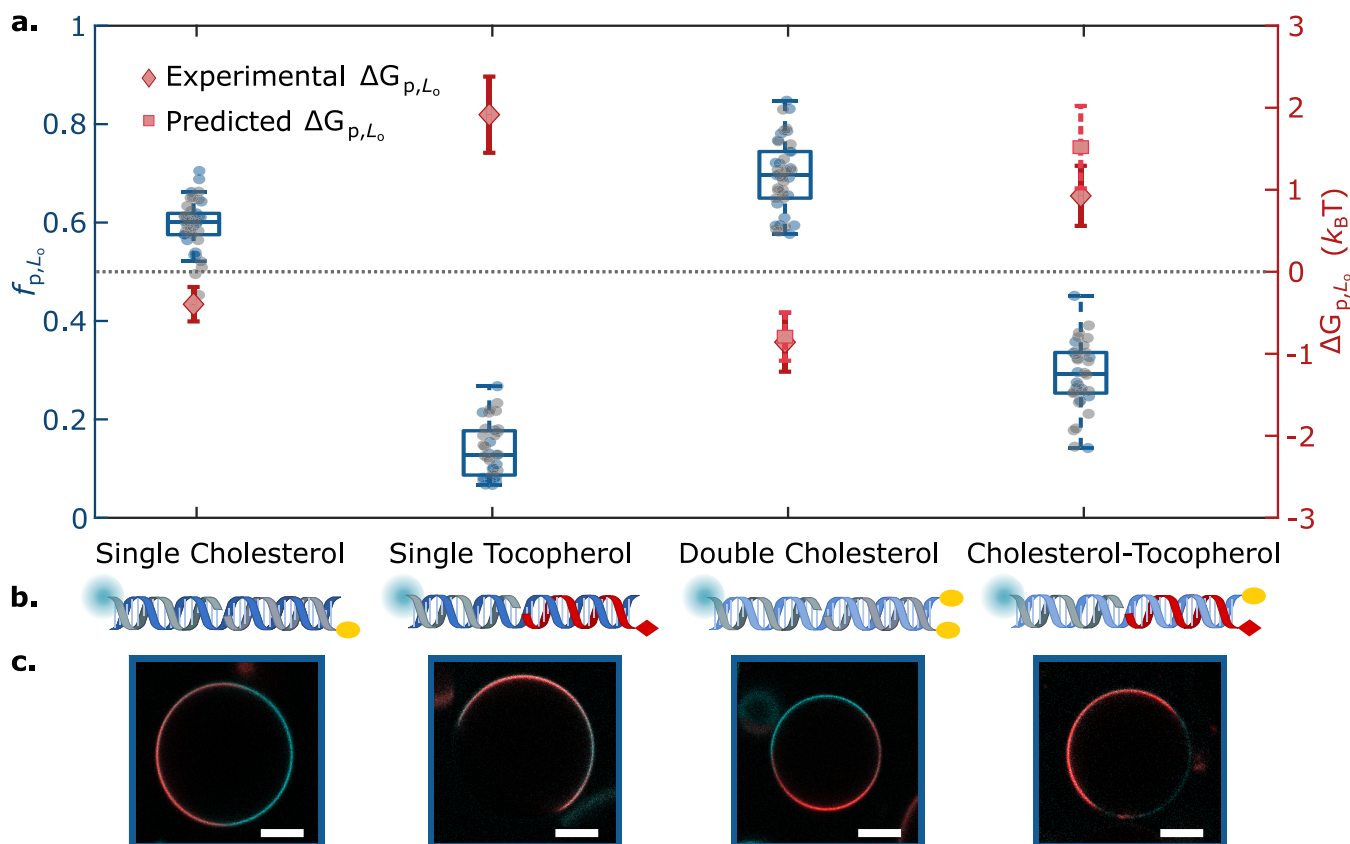


**Figure 2.** Lateral distribution of DNA nanostructures depends on anchor chemistry and combination. (a) Fractional intensity ( $f_{p,L_o}$ ) and free energy of partitioning ( $\Delta G_{p,L_o}$ ) of DNA nanostructures in  $L_o$ , conveyed by box-scatter plots and lozenges respectively, for two individual repeats (in blue/gray) of DNA-decorated GUVP populations featuring different anchoring motifs: single cholesterol-TEG (sC), double cholesterol-TEG (dC), single tocopherol (sT), or a combination of single cholesterol-TEG and single tocopherol (sC+sT). For dC and sC+sT, squares indicate the predicted free energy values for combined anchors, determined from eq 1 using measured values of  $\Delta G_{p,L_o}^{sT}$  and  $\Delta G_{p,L_o}^{sC}$ . The dotted line indicates no partitioning ( $f_{p,L_o} = 0.5$ ,  $\Delta G_{p,L_o} = 0$ ). (b) Schematic depictions of DNA duplexes bearing sC, sT, dC, or sC+sT. (c) Representative confocal micrographs of the DNA-functionalized GUVs. The  $L_d$  phase was labeled with TexasRed (red), and DNA constructs (cyan) were labeled with Alexa488. Scale bars = 10  $\mu m$ .

moieties within the same nanostructure. With this modular “mix and match” approach, we can indeed think of reinforcing partitioning in either lipid phase by increasing the number of cholesterol or tocopherol moieties on our nanodevices, or to access intermediate partitioning states with nanostructures featuring both moieties.

In the absence of (anti) co-operative effects and at sufficiently low construct concentrations, the partitioning free energy of a nanostructure featuring multiple hydrophobic moieties should be additive in the contributions from individual anchors:

$$\Delta G_{p,L_o} = \sum_i \Delta G_{p,L_o}^i \quad (1)$$

where the index  $i$  runs over all the anchors in the construct.

The simple relationship in eq 1 can guide the design of multi-anchor motifs, and in Figure 2, we tested it on a duplex featuring two cholesterol-TEG anchors (dC). As expected, the dC motif displayed an enhanced preference for  $L_o$  domains compared to sC,<sup>40,53</sup> with  $f_{p,L_o}^{dC} \approx 0.7$ . The measured partitioning free energy was  $\Delta G_{p,L_o}^{dC} \approx -0.8 k_B T$ , nearly identical to twice that of sC nanostructures. This quantitative agreement with the prediction of eq 1 suggests that, at least in this specific

case, anchor co-operativity and other nonadditive contributions negligibly affect partitioning.

When testing “chimeric” duplexes, bearing a tocopherol and a cholesterol anchor (sC+sT), we observed a pronounced preference for  $L_d$ , consistent with the expectation that tocopherol should dominate in view of the stronger free energy shift associated with its partitioning (Figure 2,  $f_{p,L_o}^{sC+sT} \approx 0.3$ ). Here, the free energy prediction from eq 1 slightly overestimated the measured value of  $\Delta G_{p,L_o}^{sC+sT} \approx 0.9 k_B T$  (statistically significant difference,  $p = 8.5 \times 10^{-11}$ , using the nonparametric Mann–Whitney Wilcoxon Test). Since this nonadditive behavior was not observed for the dC construct, we argue that it may result from the distinct chemical nature of the anchors in sC+sT and the consequent differences in their interactions with the surrounding lipids.

To further challenge our modular design approach, we studied the partitioning behavior of the constructs in Figure 2 in a quaternary lipid mixture (DOPC/DPPC/cholesterol/cardiophilin). While this more complex mixture still displayed  $L_o$ – $L_d$  phase coexistence, the incorporation of the highly unsaturated cardiophilin has been shown to enhance  $L_o$ -partitioning, owing to the increased lateral stress in the  $L_d$  phase.<sup>40</sup> The data, summarized in Figure S5, largely confirmed



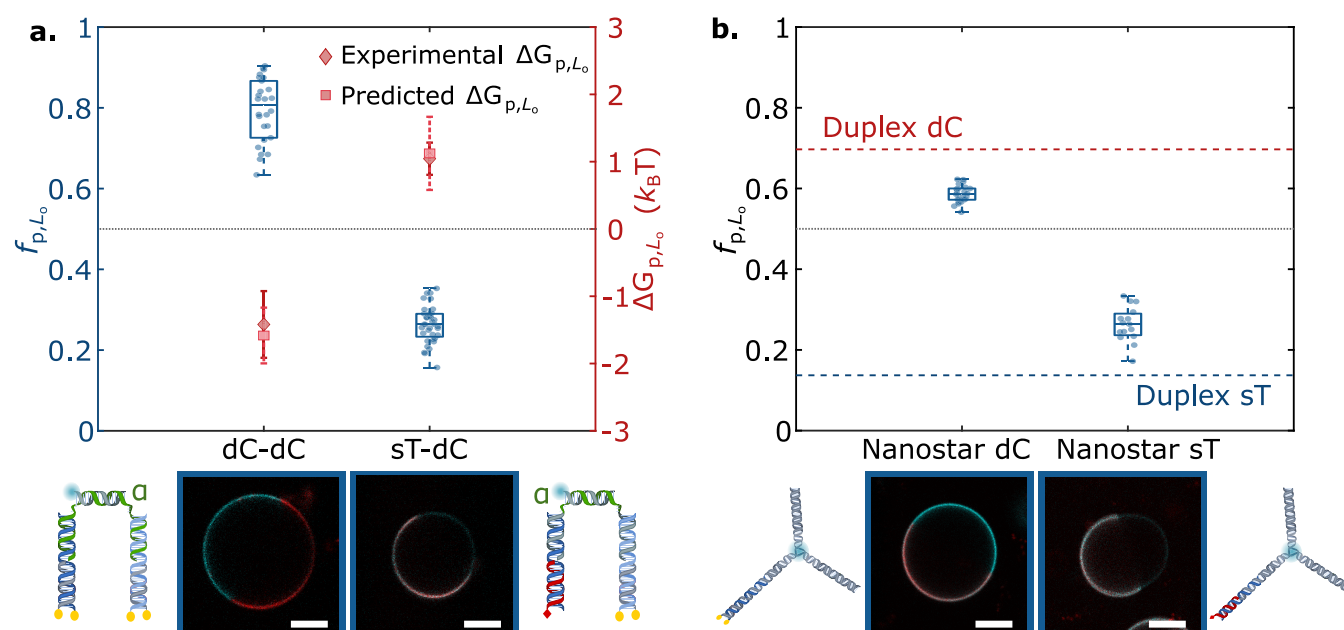


**Figure 3.** Anchor coupling and construct topology modulate DNA nanostructure partitioning. (a, top) Tunable lateral segregation of DNA architectures attained by coupling two sets of anchors: dC+dC and sT+dC. The partitioning behavior is demonstrated by the fractional intensity ( $f_{p,L_o}$ , box-scatter plots) and free energy of partitioning ( $\Delta G_{p,L_o}$ , lozenges) in  $L_o$ . Squares indicate the predicted free energy values for combined anchors, determined from eq 1 using measured values of  $\Delta G_{p,L_o}^{sT}$  and  $\Delta G_{p,L_o}^{dC}$  (Figure 2). (a, bottom) Schematic representations of the nanostructures and representative confocal micrographs of decorated GUVs. (b, top) Effect of nanostructure size on partitioning, shown via  $f_{p,L_o}$  box-scatter plots of DNA nanostars bearing single tocopherol (sT) or double-cholesterol (dC) anchors, compared against the mean  $f_{p,L_o}$  achieved by their duplex counterparts (dashed lines, red for dC, blue for sT). (b, bottom) Depiction of DNA nanostars alongside representative confocal micrographs of DNA-decorated GUVs. In plots in both panels a and b, the dotted line indicates no partitioning ( $f_{p,L_o} = 0.5$ ,  $\Delta G_{p,L_o} = 0$ ). The  $L_d$  phase was labeled with TexasRed (red), and constructs (cyan) were labeled with Alexa488 (DNA–DNA complexes) or fluorescein (nanostars). Scale bars = 10  $\mu$ m.

the predictive power of eq 1, but some nonadditive deviations are highlighted. Specifically, we observed that applying the rule in eq 1 led to an overestimation of the nanostructures' tendency to localize within the  $L_o$  for both dC and sC+sT motifs. The difference in magnitude between nonadditive free energy terms observed for ternary and quaternary lipid compositions is only partially surprising, as one would expect (anti) co-operative effects to be highly sensitive to the lipid microenvironment of the anchors. For instance, one may speculate that the cardiolipin-rich  $L_d$  phase in the quaternary mixture may be better able to accommodate larger inclusions like those generated by two-anchor motifs (dC, sC+sT), which may in turn help to relax the built-in lateral stress.<sup>40</sup> This phenomenon may lead to a less pronounced  $L_o$  preference for two-anchor compared to single-anchor constructs.

Thanks to the design freedom of DNA nanotechnology, our modular strategy is not restricted to simple motifs with one or two anchors. We can indeed regard the duplex constructs in Figure 2 as “anchoring modules” and further combine them in larger nanostructures to expand the range of accessible partitioning states. For instance, as schematically depicted in Figure 3, two anchoring modules were coupled by simply connecting them with a transversal, fluorescently labeled linker duplex. For added conformational flexibility, 3-nt single-stranded (ss)DNA domains ( $\alpha$  in Figure 3) were included between the hydrophobically modified and linker duplexes.

Two modular combinations were investigated: dC+dC and sT+dC. Notably, for both designs, the measured partitioning free energies could be quantitatively predicted by adding up the contributions of the individual anchor modules. The dC

+dC construct, as expected, displays a very strong  $L_o$  preference, with  $\Delta G_{p,L_o}^{dC+dC} \approx -1.4k_B T$  and  $f_{p,L_o}^{dC+dC} \approx 0.8$ . Similarly to the case of the sC+sT constructs, the partitioning of sT+dC nanostructures was dominated by the strong  $L_d$  preference of the tocopherol, with  $\Delta G_{p,L_o}^{sT+dC} \approx 1k_B T$  and  $f_{p,L_o}^{sT+dC} \approx 0.26$ .

Despite the remarkable accuracy of eq 1 in predicting partitioning states in multianchor constructs, we highlighted nonadditive deviations. While some of these appear to correlate with the details of anchor and lipid chemistry (sC-sT in Figure 2 and Figure S5) and are thus difficult to control, other nonadditive contributions can potentially be exploited to fine-tune partitioning states around the baseline defined by anchor combination. For instance, the use of larger and more complex nanostructures may influence lateral segregation owing to steric or electrostatic interactions between the motifs. One may indeed expect that, for larger nanostructures, excluded volume effects may hinder accumulation in one specific phase, thus suppressing partitioning. Figure 3b summarizes the partitioning behavior of three-pointed DNA nanostars anchored to the bilayers using dC and sT modules. These motifs had roughly 4 $\times$  the molecular weight of the smaller duplex architectures in Figure 2 and, indeed, systematically displayed a reduced partitioning tendency. Moreover, Figure S6 proves that the effect is not unique to the branched nanostructures, as linear duplexes anchored via dC also showed a general weakening in partitioning with increasing length. In further support to the hypothesis that steric nanostructure–nanostructure interactions may have an effect on partitioning, we performed measurements for smaller

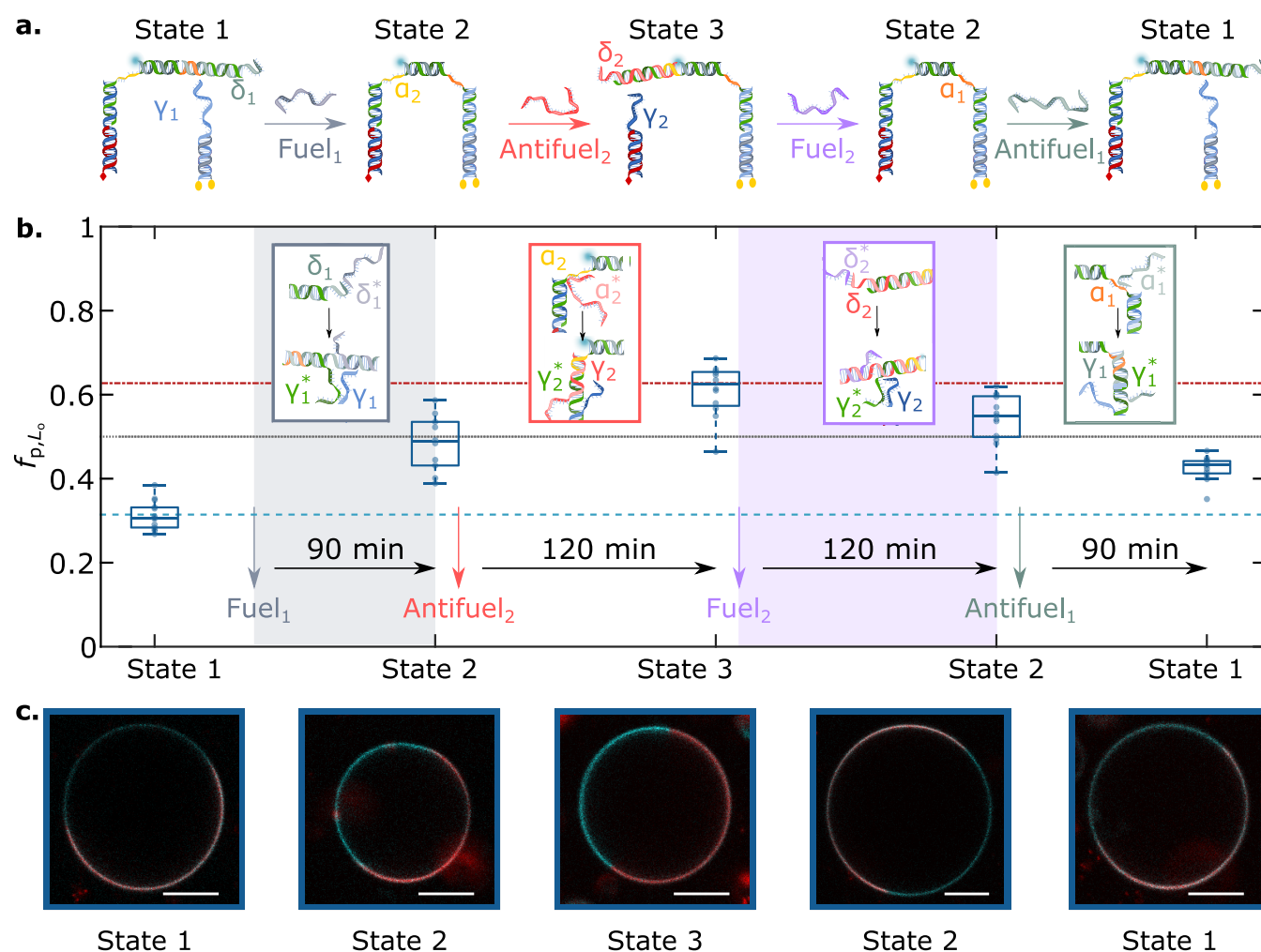


**Figure 4.** Toehold-mediated strand displacement enables cargo transport between lipid domains via lateral redistribution to programmed partitioned states: (a) Schematic depiction of the mechanism underpinning DNA nanostructure dimerization and cargo redistribution induced by the addition of Fuel/Antifuel strands, which exploit domains  $\delta_1$ ,  $\alpha_1$ ,  $\delta_2$ , and  $\alpha_2$  as toeholds. The correct response of the molecular circuit was tested with agarose gel electrophoresis, as summarized in Figure S8. (b) Evolution of the partitioning tendency of the fluorescent DNA element (panel a), conveyed by  $f_{p,L_o}$  box-scatter plots, after a delay time for equilibration upon the addition of Fuel/Antifuel strands. The light blue dashed line marks the mean  $f_{p,L_o}$  of the cargo hybridized to the sT-bearing module and in the absence of the dC-anchoring module, while the red dash-dot line marks that of the cargo hybridized to the dC-bearing module and in the absence of the sT anchoring module. The dotted line indicates no partitioning ( $f_{p,L_o} = 0.5$ ,  $\Delta G_{p,L_o} = 0$ ). (c) Representative confocal micrographs of DNA-functionalized GUVs over time, showcasing the distinct partitioned states attained by the system. The  $L_d$  phase was labeled with TexasRed (red), and DNA constructs were labeled with Alexa488 (cyan). Scale bars = 10  $\mu\text{m}$ .

dC and sT duplexes over a wide range of (nominal) DNA-to-lipid molar ratios and thus of surface densities of the motifs, as summarized in Figure S7. We observed a near stationary  $f_{p,L_o}$  over a broad range of DNA/lipid ratios around the value used for all other experiments throughout this work ( $\sim 4 \times 10^{-4}$ ). For both dC and sT constructs, however,  $f_{p,L_o}$  strongly deviated at high DNA/lipid ratios, approaching  $\sim 0.5$ . Such a deviation hints at a saturation of the  $L_o$  and  $L_d$  phases and the consequent impossibility for the nanostructures to further accumulate in those domains. Saturation occurred at higher DNA/lipid ratios for sT compared to dC, and we argue that this difference may arise from differences in the overall membrane affinity of the anchors. Indeed, while dC membrane insertion is effectively irreversible,<sup>60</sup> anchoring via sT may be weaker so that membrane-anchored sT duplexes coexist with a

larger concentration of solubilized constructs, effectively reducing the surface density at fixed DNA/lipid ratios.

Our ability to program the domain partitioning of DNA constructs by linking different anchoring modules, as demonstrated in Figure 3, can be combined with the dynamic reconfigurability of DNA nanostructures to reversibly trigger redistribution of a fluorescent cargo within the GUVs' surfaces upon exposure to molecular cues. We demonstrate this effect with a nanostructure featuring both dC and sT anchoring modules, similar to that shown in Figure 3 but in which the fluorescent dsDNA linker module (cargo) connecting the anchor duplexes can reversibly bind to or detach from either via toehold-mediated strand displacement,<sup>61</sup> a mechanism that is reminiscent of two-component biological receptors undergoing ligand-induced dimerization.<sup>5,6</sup> As sketched in Figure 4a, we initiated our system from a configuration in which the fluorescent cargo was attached to the sT anchor and thus

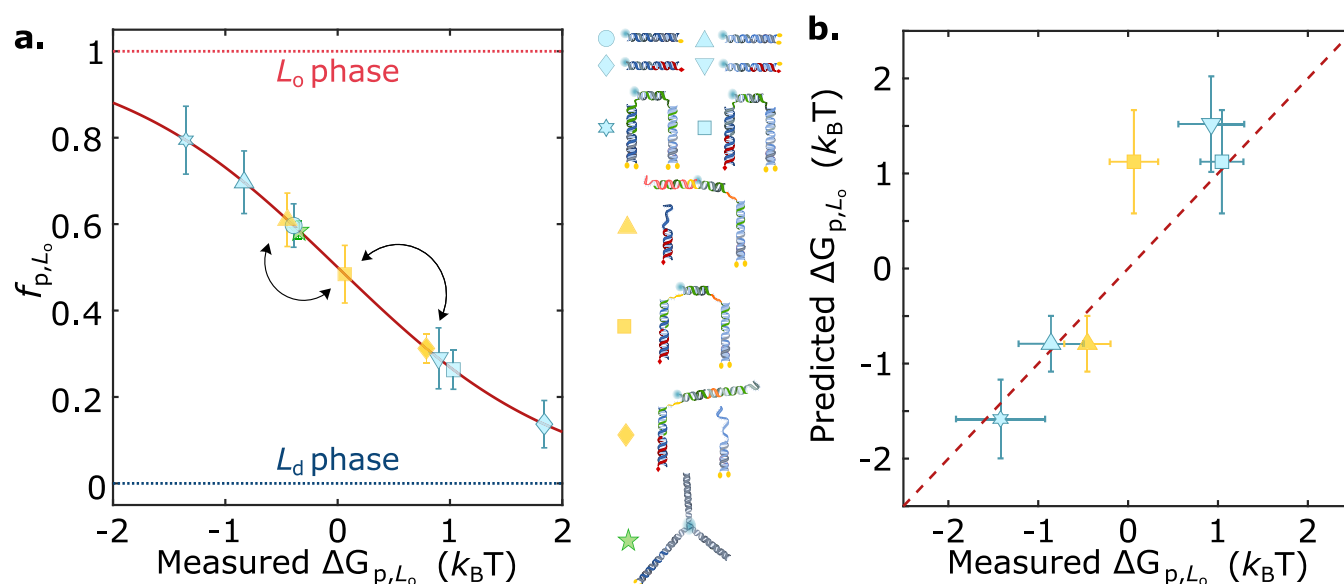


**Figure 5.** Static and dynamic engineering of partitioning states across the free-energy landscape by prescribing anchor combination and nanostructure morphology. (a) Summary graph demonstrating the mean  $f_{p,L_o} \pm$  standard deviations of several membrane-associated DNA nanostructures as a function of their measured free energy of partitioning ( $\Delta G_{p,L_o}$ ). The effect of anchor coupling, size, and geometry is showcased. Arrows connect programmed partitioned states achieved by the responsive nanodevice discussed in Figure 4. (b) Partitioning free energy of DNA nanostructures is to a good approximation additive in contributions from individual anchoring motifs, as shown for several multianchor nanostructures with the mean  $\pm$  standard deviations of measured  $\Delta G_{p,L_o}$  vs those predicted with eq 1.

localized in the  $L_d$  phase (State 1). Here, the fluorescent linker module was prevented from connecting to the dC anchoring module as its domain  $\gamma_1^*$ , complementary to  $\gamma_1$  on the dC module, was protected by an Antifuel<sub>1</sub> strand of domain sequence  $\delta_1\gamma_1\alpha_1^*$ . Note that the  $f_{p,L_o}$  value recorded in this configuration matched exactly the one measured if the dC module was absent from the bilayer, marked by a dashed line in Figure 4b, thus confirming the absence of binding to the dC module. Antifuel<sub>1</sub> could be displaced upon addition of Fuel<sub>1</sub>, leading to the exposure of  $\gamma_1^*$  on the linker module and its binding to the dC module. Upon acquiring this configuration, State 2, the nanostructures shifted the cargo toward  $L_o$ . Addition of Antifuel<sub>2</sub>, with sequence  $\alpha_2^*\gamma_2\delta_2$ , triggered the displacement of the linker from the sT module following a toehold reaction initiated at domain  $\alpha_2$ , leading to the emergence of State 3 and a further cargo redistribution toward the  $L_o$  phase. Also in this configuration, the  $f_{p,L_o}$  value aligned to that measured in the absence of sT anchors, indicating a near-complete progression of the toehold reaction (dot-dash line in Figure 4b). Finally, sequential addition of Fuel<sub>2</sub> and Antifuel<sub>1</sub> could reverse the systems' configuration to States 2 and then 1. The last two steps pushed the fluorescent cargo back toward its initial  $L_d$  preference, but the  $f_{p,L_o}$  values remained slightly higher than those recorded at first. This incomplete reversibility may be due to partial inefficiencies in the reverse toehold reactions<sup>62</sup> or to a small thermodynamic unbalance that favors State 3 over State 1. Note that the system was allowed to fully equilibrate after the addition of fuel/antifuel strands prior to collecting the data in Figure 4, as demonstrated by the measurements acquired at intermediate time points and shown in Figure S9a. In turn, Figure S9b shows the time evolution of  $f_{p,L_o}$  for an individual GUV, in which the nanostructures transition from State 1 to State 2 upon fuel addition. The equilibration time scales of  $\sim 5$  min are

likely limited by the diffusion of the fuel strand through the sample, given that, in order to prevent GUV drift and disruption, the fuel solution is gently added from the sample surface without any active mixing. The rates of toehold-mediated strand displacement and diffusion of the membrane-anchored constructs are expected to be comparatively faster (see discussion in the caption of Figure S9). The redistribution recorded for our nanodevices is comparable to those of biological membrane-anchored agents involved, for example, in the recruitment of receptors upon T-cell activation<sup>63</sup> or clathrin-mediated endocytosis,<sup>8,64</sup> both of which range between tens and hundreds of seconds. Finally, note that States 1 and 3 displayed a lower tendency to partition in  $L_d$  and  $L_o$  (respectively) compared to their sT and dC duplex analogues (Figure 2). The shift is likely a consequence of the greater steric encumbrance of the responsive motifs, discussed above with respect to Figure 3 and Figure S6.

In summary, we introduced a modular approach to engineer the lateral distribution of amphiphilic DNA nanostructures between coexisting phases of synthetic membranes. We exploited the ability of individual cholesterol and tocopherol anchors to induce partitioning in  $L_o$  and  $L_d$ , respectively, and combined them to produce an array of multianchor nanodevices that span a broad range of partitioning behaviors from  $\sim 80\%$  preference for  $L_o$  to  $\sim 85\%$  partitioning in  $L_d$ , as summarized in Figure 5a. The comparison between measured partitioning free energies and those extracted from eq 1, shown in Figure 5b, proves that to a good approximation  $\Delta G_{p,L_o}$  is additive in the contributions from individual anchors, thus offering a predictive design criterion. Small, nonadditive effects contribute to a different extent depending on anchor combinations and lipid-membrane composition, hinting at (anti) co-operative effects dependent on system-specific chemistry, while excluded-volume effects emerged for bulkier motifs and higher nanostructure concentrations.



The modularity of our design strategy enables dynamic control over the partitioning state by altering the anchor makeup of the nanostructures, as we showed with a proof-of-concept experiment in which fluorescent cargoes were reversibly transported across vesicle surfaces upon exposure to molecular cues. This strategy evokes that used by cells to control spatiotemporal localization of membrane proteins<sup>47–49,65</sup> and can be further extended to respond to other physico-chemical triggers by including stimuli-sensitive motifs such as aptamers,<sup>66</sup> DNazymes,<sup>67</sup> G-quadruplexes,<sup>68</sup> pH-responsive motifs,<sup>69</sup> and other functional DNA architectures.<sup>70,71</sup>

Our approach could be easily extended to include moieties other than cholesterol and tocopherol, such as alkyl chains,<sup>40</sup> porphyrin,<sup>72</sup> and azobenzene,<sup>73</sup> which besides unlocking a broader range of partitioning states may also enable responsiveness to a wider spectrum of stimuli. Similar design principles could even be applied to membrane-associated entities different from (amphiphilic) DNA nanostructures, such as peripheral and integral proteins, to program their colocalization in membrane domains.<sup>74,75</sup>

Our platform paves the way for the development of next-generation biomimetic DNA devices for the bottom-up engineering of life-like behaviors in synthetic cellular systems, which could in the long term find application in high-tech therapeutics and diagnostic solutions. For instance, the stimuli-triggered reshuffling of membrane-bound objects between lipid phases can enable highly sought behaviors such as signal transduction, communication, and local membrane sculpting.<sup>45</sup> Examples include stimuli-induced colocalization of *synthetic receptors* initiating artificial signaling cascades<sup>44</sup> and herding of objects capable of influencing local membrane curvature, thus directing morphological restructuring such as tubular growth<sup>76</sup> and exosome/endosome budding.<sup>46,77,78</sup>

## ■ ASSOCIATED CONTENT

### Supporting Information

The Supporting Information is available free of charge at <https://pubs.acs.org/doi/10.1021/acs.nanolett.0c04867>.

Experimental methods, discussion of impact of fluorescence cross-talk and FRET, image analysis pipeline for measuring DNA-construct fluorescence intensity in equatorial confocal micrographs, circle fitting routine to correct for imperfect segmentation of low intensity equatorial membrane domains, impact of fluorescent lipid marker and GUV polydispersity on partitioning tendency, lateral distribution of duplex DNA nanostructures in quaternary (DOPC/DPPC/cardiophospholipin/chol) GUVs, lateral distribution of DNA nanostructures of increasing molecular weight, suppression of partitioning by high DNA/lipid ratio due to membrane saturation, DNA nanostructure reconfigurability via toehold reactions, DNA nanostructure reconfiguration and redistribution, and DNA sequences of the nanostructures used throughout this work (PDF)

## ■ AUTHOR INFORMATION

### Corresponding Author

**Lorenzo Di Michele** – Biological and Soft Systems, Cavendish Laboratory, University of Cambridge, Cambridge CB3 0HE, United Kingdom; Molecular Sciences Research Hub, Department of Chemistry, Imperial College London, London

W12 0BZ, United Kingdom; [orcid.org/0000-0002-1458-9747](https://orcid.org/0000-0002-1458-9747); Email: [l.di-michele@imperial.ac.uk](mailto:l.di-michele@imperial.ac.uk)

### Authors

**Roger Rubio-Sánchez** – Biological and Soft Systems, Cavendish Laboratory, University of Cambridge, Cambridge CB3 0HE, United Kingdom; [orcid.org/0000-0001-5574-5809](https://orcid.org/0000-0001-5574-5809)

**Simone Eizagirre Barker** – Biological and Soft Systems, Cavendish Laboratory, University of Cambridge, Cambridge CB3 0HE, United Kingdom; [orcid.org/0000-0001-8920-0428](https://orcid.org/0000-0001-8920-0428)

**Michał Walczak** – Biological and Soft Systems, Cavendish Laboratory, University of Cambridge, Cambridge CB3 0HE, United Kingdom

**Pietro Cicuta** – Biological and Soft Systems, Cavendish Laboratory, University of Cambridge, Cambridge CB3 0HE, United Kingdom; [orcid.org/0000-0002-9193-8496](https://orcid.org/0000-0002-9193-8496)

Complete contact information is available at: <https://pubs.acs.org/doi/10.1021/acs.nanolett.0c04867>

### Notes

The authors declare no competing financial interest.

## ■ ACKNOWLEDGMENTS

R.R.S. acknowledges support from the Mexican National Council for Science and Technology (CONACYT, Grant No. 472427) and the Cambridge Trust. R.R.S. and S.E.B. also acknowledge funding from the EPSRC CDT in Nanoscience and Nanotechnology (NanoDTC, Grant No. EP/L015978/1 and EP/S022953/1, respectively). L.D.M. acknowledges funding from a Royal Society University Research Fellowship (UF160152) and from the European Research Council (ERC) under the Horizon 2020 Research and Innovation Programme (ERC-STG No 851667 NANOCELL). The authors thank B. M. Moggetti for discussions on the project, and D. Morzy for comments on the manuscript. All data in support of this work can be accessed free of charge at <https://doi.org/10.17863/CAM.64579>.

## ■ REFERENCES

- (1) Heberle, F. A.; Feigenson, G. W. Phase Separation in Lipid Membranes. *Cold Spring Harbor Perspectives in Biology* **2011**, 3, No. a004630.
- (2) Lorent, J. H.; Levental, K. R.; Ganesan, L.; Rivera-Longworth, G.; Sezgin, E.; Doktorova, M.; Lyman, E.; Levental, I. Plasma membranes are asymmetric in lipid unsaturation, packing and protein shape. *Nat. Chem. Biol.* **2020**, 16, 644–652.
- (3) Alberts, B. *Molecular biology of the cell*, 6th ed.; Garland Science: New York, 2017.
- (4) Sezgin, E.; Levental, I.; Mayor, S.; Eggeling, C. The mystery of membrane organization: composition, regulation and roles of lipid rafts. *Nat. Rev. Mol. Cell Biol.* **2017**, 18, 361–374.
- (5) Akira, S.; Takeda, K. Toll-like receptor signalling. *Nat. Rev. Immunol.* **2004**, 4, 499.
- (6) Schlessinger, J. Receptor Tyrosine Kinases: Legacy of the First Two Decades. *Cold Spring Harbor Perspect. Biol.* **2014**, 6, No. a008912.
- (7) Acebrón, I.; et al. Structural basis of Focal Adhesion Kinase activation on lipid membranes. *EMBO Journal* **2020**, 39, No. e104743.
- (8) Haucke, V.; Kozlov, M. M. Membrane remodeling in clathrin-mediated endocytosis. *J. Cell Sci.* **2018**, 131, No. jcs216812.
- (9) Stoten, C. L.; Carlton, J. G. ESCRT-dependent control of membrane remodelling during cell division. *Semin. Cell Dev. Biol.* **2018**, 74, 50–65.

- (10) Veatch, S. L.; Cicuta, P. In *Critical Lipidomics: The Consequences of Lipid Miscibility in Biological Membranes BT - Physics of Biological Membranes*; Bassereau, P., Sens, P., Eds.; Springer International Publishing: Cham, 2018; pp 141–168.
- (11) McMahon, H. T.; Gallop, J. L. Membrane curvature and mechanisms of dynamic cell membrane remodelling. *Nature* **2005**, *438*, 590–596.
- (12) Baumgart, T.; Capraro, B. R.; Zhu, C.; Das, S. L. Thermodynamics and Mechanics of Membrane Curvature Generation and Sensing by Proteins and Lipids. *Annu. Rev. Phys. Chem.* **2011**, *62*, 483–506.
- (13) Pike, L. J. Lipid rafts: bringing order to chaos. *J. Lipid Res.* **2003**, *44*, 655–667.
- (14) Pralle, A.; Keller, P.; Florin, E.-L.; Simons, K.; Hörber, J. K. H. Sphingolipid-Cholesterol Rafts Diffuse as Small Entities in the Plasma Membrane of Mammalian Cells. *J. Cell Biol.* **2000**, *148*, 997–1008.
- (15) Lingwood, D.; Simons, K. Lipid Rafts As a Membrane-Organizing Principle. *Science* **2010**, *327*, 46–50.
- (16) Buddingh', B. C.; van Hest, J. C. M. Artificial Cells: Synthetic Compartments with Life-like Functionality and Adaptivity. *Acc. Chem. Res.* **2017**, *50*, 769–777.
- (17) Noireaux, V.; Libchaber, A. A vesicle bioreactor as a step toward an artificial cell assembly. *Proc. Natl. Acad. Sci. U. S. A.* **2004**, *101*, 17669–17674.
- (18) Noireaux, V.; Maeda, Y. T.; Libchaber, A. Development of an artificial cell, from self-organization to computation and self-reproduction. *Proc. Natl. Acad. Sci. U. S. A.* **2011**, *108*, 3473–3480.
- (19) Elani, Y. Construction of membrane-bound artificial cells using microfluidics: a new frontier in bottom-up synthetic biology. *Biochem. Soc. Trans.* **2016**, *44*, 723–730.
- (20) Karamdad, K.; Hindley, J. W.; Bolognesi, G.; Friddin, M. S.; Law, R. V.; Brooks, N. J.; Ces, O.; Elani, Y. Engineering thermoresponsive phase separated vesicles formed via emulsion phase transfer as a content-release platform. *Chemical Science* **2018**, *9*, 4851–4858.
- (21) Trantidou, T.; Friddin, M.; Elani, Y.; Brooks, N. J.; Law, R. V.; Seddon, J. M.; Ces, O. Engineering Compartmentalized Biomimetic Micro- and Nanocontainers. *ACS Nano* **2017**, *11*, 6549–6565.
- (22) Choi, H.-J.; Brooks, E.; Montemagno, C. D. Synthesis and characterization of nanoscale biomimetic polymer vesicles and polymer membranes for bioelectronic applications. *Nanotechnology* **2005**, *16*, S143–S149.
- (23) Joesaar, A.; Yang, S.; Bögers, B.; van der Linden, A.; Pieters, P.; Kumar, B. V. S. P.; Dalchau, N.; Phillips, A.; Mann, S.; de Greef, T. F. A. DNA-based communication in populations of synthetic protocells. *Nat. Nanotechnol.* **2019**, *14*, 369–378.
- (24) Ugrinic, M.; Zambrano, A.; Berger, S.; Mann, S.; Tang, T.-Y. D.; DeMello, A. Microfluidic formation of proteinosomes. *Chem. Commun.* **2018**, *54*, 287–290.
- (25) Li, M.; Harbron, R. L.; Weaver, J. V. M.; Binks, B. P.; Mann, S. Electrostatically gated membrane permeability in inorganic protocells. *Nat. Chem.* **2013**, *5*, 529–536.
- (26) Li, M.; Green, D. C.; Anderson, J. L. R.; Binks, B. P.; Mann, S. In vitro gene expression and enzyme catalysis in bio-inorganic protocells. *Chem. Sci.* **2011**, *2*, 1739–1745.
- (27) Hindley, J. W.; Zheleva, D. G.; Elani, Y.; Charalambous, K.; Barter, L. M. C.; Booth, P. J.; Bevan, C. L.; Law, R. V.; Ces, O. Building a synthetic mechanosensitive signaling pathway in compartmentalized artificial cells. *Proc. Natl. Acad. Sci. U. S. A.* **2019**, *116*, 16711–16716.
- (28) Altamura, E.; Milano, F.; Tangorra, R. R.; Trotta, M.; Omar, O. H.; Stano, P.; Mavelli, F. Highly oriented photosynthetic reaction centers generate a proton gradient in synthetic protocells. *Proc. Natl. Acad. Sci. U. S. A.* **2017**, *114*, 3837–3842.
- (29) Litschel, T.; Ramm, B.; Maas, R.; Heymann, M.; Schwill, P. Beating Vesicles: Encapsulated Protein Oscillations Cause Dynamic Membrane Deformations. *Angew. Chem., Int. Ed.* **2018**, *57*, 16286–16290.
- (30) Hindley, J. W.; Elani, Y.; McGilvery, C. M.; Ali, S.; Bevan, C. L.; Law, R. V.; Ces, O. Light-triggered enzymatic reactions in nested vesicle reactors. *Nat. Commun.* **2018**, *9*, 1093.
- (31) Lee, K. Y.; Park, S.-J.; Lee, K. A.; Kim, S.-H.; Kim, H.; Meroz, Y.; Mahadevan, L.; Jung, K.-H.; Ahn, T. K.; Parker, K. K.; Shin, K. Photosynthetic artificial organelles sustain and control ATP-dependent reactions in a protocellular system. *Nat. Biotechnol.* **2018**, *36*, 530–535.
- (32) Hindley, J. W.; Law, R. V.; Ces, O. Membrane functionalization in artificial cell engineering. *SN Applied Sciences* **2020**, *2*, 593.
- (33) Seeman, N. C.; Sleiman, H. F. DNA nanotechnology. *Nature Reviews Materials* **2018**, *3*, 17068.
- (34) Zhao, N.; Chen, Y.; Chen, G.; Xiao, Z. Artificial Cells Based on DNA Nanotechnology. *ACS Applied Bio Materials* **2020**, *3*, 3928–3934.
- (35) Moggetti, B. M.; Cicuta, P.; Di Michele, L. Programmable interactions with biomimetic DNA linkers at fluid membranes and interfaces. *Rep. Prog. Phys.* **2019**, *82*, 116601.
- (36) Amjad, O. A.; Moggetti, B. M.; Cicuta, P.; Di Michele, L. Membrane Adhesion through Bridging by Multimeric Ligands. *Langmuir* **2017**, *33*, 1139–1146.
- (37) Bachmann, S. J.; Kotar, J.; Parolini, L.; Šarić, A.; Cicuta, P.; Di Michele, L.; Moggetti, B. M. Melting transition in lipid vesicles functionalised by mobile DNA linkers. *Soft Matter* **2016**, *12*, 7804–7817.
- (38) Parolini, L.; Moggetti, B. M.; Kotar, J.; Eiser, E.; Cicuta, P.; Di Michele, L. Volume and porosity thermal regulation in lipid mesophases by coupling mobile ligands to soft membranes. *Nat. Commun.* **2015**, *6*, 5948.
- (39) Parolini, L.; Kotar, J.; Di Michele, L.; Moggetti, B. M. Controlling Self-Assembly Kinetics of DNA-Functionalized Liposomes Using Toehold Exchange Mechanism. *ACS Nano* **2016**, *10*, 2392–2398.
- (40) Beales, P. A.; Nam, J.; Vanderlick, T. K. Specific adhesion between DNA-functionalized “Janus” vesicles: size-limited clusters. *Soft Matter* **2011**, *7*, 1747–1755.
- (41) Beales, P. A.; Vanderlick, T. K. DNA as Membrane-Bound Ligand-Receptor Pairs: Duplex Stability Is Tuned by Intermembrane Forces. *Biophys. J.* **2009**, *96*, 1554–1565.
- (42) Burns, J. R.; Seifert, A.; Fertig, N.; Howorka, S. A biomimetic DNA-based channel for the ligand-controlled transport of charged molecular cargo across a biological membrane. *Nat. Nanotechnol.* **2016**, *11*, 152.
- (43) Göpfrich, K.; Li, C.-Y.; Mames, I.; Bhamidimarri, S. P.; Ricci, M.; Yoo, J.; Mames, A.; Ohmann, A.; Winterhalter, M.; Stulz, E.; Aksimentiev, A.; Keyser, U. F. Ion Channels Made from a Single Membrane-Spanning DNA Duplex. *Nano Lett.* **2016**, *16*, 4665–4669.
- (44) Kaufhold, W. T.; Brady, R. A.; Tuffnell, J. M.; Cicuta, P.; Di Michele, L. Membrane Scaffolds Enhance the Responsiveness and Stability of DNA-Based Sensing Circuits. *Bioconjugate Chem.* **2019**, *30*, 1850–1859.
- (45) Franquelim, H. G.; Khmelinskaya, A.; Sobczak, J.-P.; Dietz, H.; Schwill, P. Membrane sculpting by curved DNA origami scaffolds. *Nat. Commun.* **2018**, *9*, 811.
- (46) Journot, C. M. A.; Ramakrishna, V.; Wallace, M. I.; Turberfield, A. J. Modifying Membrane Morphology and Interactions with DNA Origami Clathrin-Mimic Networks. *ACS Nano* **2019**, *13*, 9973–9979.
- (47) Wang, T.-Y.; Leventis, R.; Silvius, J. R. Partitioning of Lipidated Peptide Sequences into Liquid-Ordered Lipid Domains in Model and Biological Membranes. *Biochemistry* **2001**, *40*, 13031–13040.
- (48) Weise, K.; Triola, G.; Janosch, S.; Waldmann, H.; Winter, R. Visualizing association of lipidated signaling proteins in heterogeneous membranes Partitioning into subdomains, lipid sorting, interfacial adsorption, and protein association. *Biochim. Biophys. Acta, Biomembr.* **2010**, *1798*, 1409–1417.
- (49) Weise, K.; Kapoor, S.; Denter, C.; Nikolaus, J.; Opitz, N.; Koch, S.; Triola, G.; Herrmann, A.; Waldmann, H.; Winter, R. Membrane-Mediated Induction and Sorting of K-Ras Microdomain Signaling Platforms. *J. Am. Chem. Soc.* **2011**, *133*, 880–887.



- (50) Beales, P. A.; Vanderlick, T. K. Application of nucleic acid-lipid conjugates for the programmable organisation of liposomal modules. *Adv. Colloid Interface Sci.* **2014**, *207*, 290–305.
- (51) Veatch, S. L.; Keller, S. L. Separation of Liquid Phases in Giant Vesicles of Ternary Mixtures of Phospholipids and Cholesterol. *Biophys. J.* **2003**, *85*, 3074–3083.
- (52) Veatch, S. L.; Keller, S. L. Miscibility Phase Diagrams of Giant Vesicles Containing Sphingomyelin. *Phys. Rev. Lett.* **2005**, *94*, 148101.
- (53) Beales, P. A.; Vanderlick, T. K. Partitioning of Membrane-Anchored DNA between Coexisting Lipid Phases. *J. Phys. Chem. B* **2009**, *113*, 13678–13686.
- (54) Talbot, E. L.; Parolini, L.; Kotar, J.; Di Michele, L.; Cicuta, P. Thermal-driven domain and cargo transport in lipid membranes. *Proc. Natl. Acad. Sci. U. S. A.* **2017**, *114*, 846–851.
- (55) Bunge, A.; Kurz, A.; Windeck, A.-K.; Korte, T.; Flasche, W.; Liebscher, J.; Herrmann, A.; Huster, D. Lipophilic Oligonucleotides Spontaneously Insert into Lipid Membranes, Bind Complementary DNA Strands, and Sequester into Lipid-Disordered Domains. *Langmuir* **2007**, *23*, 4455–4464.
- (56) Kurz, A.; Bunge, A.; Windeck, A.-K.; Rost, M.; Flasche, W.; Arbuzova, A.; Strohbach, D.; Müller, S.; Liebscher, J.; Huster, D.; Herrmann, A. Lipid-Anchored Oligonucleotides for Stable Double-Helix Formation in Distinct Membrane Domains. *Angew. Chem., Int. Ed.* **2006**, *45*, 4440–4444.
- (57) Schade, M.; Knoll, A.; Vogel, A.; Seitz, O.; Liebscher, J.; Huster, D.; Herrmann, A.; Arbuzova, A. Remote Control of Lipophilic Nucleic Acids Domain Partitioning by DNA Hybridization and Enzymatic Cleavage. *J. Am. Chem. Soc.* **2012**, *134*, 20490–20497.
- (58) Czogalla, A.; Petrov, E. P.; Kauert, D. J.; Uzunova, V.; Zhang, Y.; Seidel, R.; Schwille, P. Switchable domain partitioning and diffusion of DNA origami rods on membranes. *Faraday Discuss.* **2013**, *161*, 31–43.
- (59) Schindelin, J.; et al. Fiji: an open-source platform for biological-image analysis. *Nat. Methods* **2012**, *9*, 676–682.
- (60) Pfeiffer, I.; Höök, F. Bivalent Cholesterol-Based Coupling of Oligonucleotides to Lipid Membrane Assemblies. *J. Am. Chem. Soc.* **2004**, *126*, 10224–10225.
- (61) Zhang, D. Y.; Winfree, E. Control of DNA Strand Displacement Kinetics Using Toehold Exchange. *J. Am. Chem. Soc.* **2009**, *131*, 17303–17314.
- (62) Chen, R. P.; Blackstock, D.; Sun, Q.; Chen, W. Dynamic protein assembly by programmable DNA strand displacement. *Nat. Chem.* **2018**, *10*, 474–481.
- (63) Bini, L.; Pacini, S.; Liberatori, S.; Valensin, S.; Pellegrini, M.; Raggiaschi, R.; Pallini, V.; Baldari, C. T. Extensive temporally regulated reorganization of the lipid raft proteome following T-cell antigen receptor triggering. *Biochem. J.* **2003**, *369*, 301–309.
- (64) Taylor, M. J.; Perrais, D.; Merrifield, C. J. A High Precision Survey of the Molecular Dynamics of Mammalian Clathrin-Mediated Endocytosis. *PLoS Biol.* **2011**, *9*, No. e1000604.
- (65) Rocks, O.; Peyker, A.; Bastiaens, P. I. H. Spatio-temporal segregation of Ras signals: one ship, three anchors, many harbors. *Curr. Opin. Cell Biol.* **2006**, *18*, 351–357.
- (66) Del Grosso, E.; Ragazzon, G.; Prins, L. J.; Ricci, F. Back Cover: Fuel-Responsive Allosteric DNA-Based Aptamers for the Transient Release of ATP and Cocaine (Angew. Chem. Int. Ed. 17/2019). *Angew. Chem., Int. Ed.* **2019**, *58*, 5772.
- (67) Lu, Y.; Liu, J. Functional DNA nanotechnology: emerging applications of DNazymes and aptamers. *Curr. Opin. Biotechnol.* **2006**, *17*, 580–588.
- (68) Cozzoli, L.; Gjonaj, L.; Stuart, M. C. A.; Poolman, B.; Roelfes, G. Responsive DNA G-quadruplex micelles. *Chem. Commun.* **2018**, *54*, 260–263.
- (69) Idili, A.; Vallée-Bélisle, A.; Ricci, F. Programmable pH-Triggered DNA Nanoswitches. *J. Am. Chem. Soc.* **2014**, *136*, 5836–5839.
- (70) Ma, L.; Liu, J. Catalytic Nucleic Acids: Biochemistry, Chemical Biology, Biosensors, and Nanotechnology. *iScience* **2020**, *23*, 100815.
- (71) Le Vay, K.; Salibi, E.; Song, E. Y.; Mutschler, H. Nucleic Acid Catalysis under Potential Prebiotic Conditions. *Chem. - Asian J.* **2020**, *15*, 214–230.
- (72) Burns, J. R.; Göpfrich, K.; Wood, J. W.; Thacker, V. V.; Stulz, E.; Keyser, U. F.; Howorka, S. Lipid-Bilayer-Spanning DNA Nanopores with a Bifunctional Porphyrin Anchor. *Angew. Chem., Int. Ed.* **2013**, *52*, 12069–12072.
- (73) Hernández-Ainsa, S.; Ricci, M.; Hilton, L.; Aviñó, A.; Eritja, R.; Keyser, U. F. Controlling the Reversible Assembly of Liposomes through a Multistimuli Responsive Anchored DNA. *Nano Lett.* **2016**, *16*, 4462–4466.
- (74) Lorent, J. H.; Diaz-Rohrer, B.; Lin, X.; Spring, K.; Gorge, A. A.; Levental, K. R.; Levental, I. Structural determinants and functional consequences of protein affinity for membrane rafts. *Nat. Commun.* **2017**, *8*, 1219.
- (75) Lin, X.; Gorge, A. A.; Levental, I. Protein Partitioning into Ordered Membrane Domains: Insights from Simulations. *Biophys. J.* **2018**, *114*, 1936–1944.
- (76) Talbot, E. L.; Kotar, J.; Di Michele, L.; Cicuta, P. Directed tubule growth from giant unilamellar vesicles in a thermal gradient. *Soft Matter* **2019**, *15*, 1676–1683.
- (77) Booth, A.; Marklew, C. J.; Ciani, B.; Beales, P. A. In Vitro Membrane Remodeling by ESCRT is Regulated by Negative Feedback from Membrane Tension. *iScience* **2019**, *15*, 173–184.
- (78) Booth, A.; Marklew, C.; Ciani, B.; Beales, P. A. The influence of phosphatidylserine localisation and lipid phase on membrane remodelling by the ESCRT-II/ESCRT-III complex. *Faraday Discuss.* **2020**, DOI: 10.1039/D0FD00042F.